Vortex Generator Jet Flow Control in Highly Loaded Compressors

João Carvalho Baiense Jr.

A Thesis
Submitted to the Faculty
of the
WORCESTER POLYTECHNIC INSTITUTE
in partial fulfillment of the requirements for the
Degree of Master of Science
in
Mechanical Engineering

June 2014

Vortex Generator Jet Flow Control in Highly Loaded Compressors

João Carvalho Baiense Jr.

A Thesis
Submitted to the Faculty
of the
WORCESTER POLYTECHNIC INSTITUTE
in partial fulfillment of the requirements for the
Degree of Master of Science
in
Mechanical Engineering
June 2014

João Carvalho Baiense Jr.

Simon W. Evans, Thesis Advisor

David Olinger, Thesis Committee

John Blandino, Thesis Committee

Mark Richman, Graduate Committee Representative

Dedicado à minha família
João, Ruth e Diana

Abstract

A flow control method for minimizing losses in a highly loaded compressor blade was analyzed. Passive and active flow control experiments with vortex generator jets were conducted on a seven blade linear compressor cascade to demonstrate the potential application of passive flow control on a highly loaded blade. Passive flow control vortex generator jets use the pressure distribution generated by air flow over the blade profile to drive jets from the pressure side to the suction side. Active flow control was analyzed by pressuring the blade plenum with an auxiliary compressor unit. Active flow control decreased profile losses by approximately 37 % while passive flow control had negligible impact on the profile loss of a highly loaded blade. Passive flow control was able to achieve a jet velocity ratio, jet velocity to upstream velocity, of 0.525. The success of active flow control with a velocity ratio of 0.9 suggests there is potential for passive flow control to be effective. The research presented in this thesis is motivated by the potential savings in the applications of passive flow control in gas turbine axial compressors by increasing the aerodynamic load of each stage. Increased stage loading that is properly controlled can reduce the number of stages required to achieve the desired pressure compression ratio.

Acknowledgements

I would like to acknowledge my loving parents, João and Ruth Baiense, for everything they have done for me. Fourteen years ago they migrated to the U.S. in search of a better life and educational opportunities for me. They encouraged me to pursue scholastic endeavors allowing me to become the first person in our family to graduate from college. I cannot thank them enough for all their hard work, dedication, and for being the most amazing and loving parents.

I would like to thank my advisor and mentor, Simon Evans, for his continual guidance in this research project. Simon fostered an environment of intellectual curiosity allowing me to explore the concepts and areas of my personal interest. From the courses he taught to the personal interaction with his students, Simon treated everyone with respect and tact always finding the best manner in which to encourage students. I have learned so much from him in these last 3 years and am very grateful for having the opportunity to work with him.

I also acknowledge the faculty members that have served as part of the thesis committee. I've had the opportunity to interact with each of them through courses and projects over my various years at WPI and I'm very thankful for their willingness to help students and for their support.

I also acknowledge my girlfriend for always supporting me through the good and difficult times. Thank you for all those late night phone calls as I drove home from the lab, for listening to all the difficulties I had and most importantly, thanks for all the prayers.

I also acknowledge Professor John Hall for allowing me to borrow noise canceling headphones for the long hours of running the wind tunnel.

I also acknowledge Peter Hefti and Randy Robinson who assisted with troubleshooting hardware related issues.

I also acknowledge the Barbara Edilberti, Barbara Furhman and Statia Canning for being so kind and helpful with scheduling, purchasing and issues related to my degree requirements. They always went over and above their job description to help.

I also acknowledge the various undergraduate teams who have contributed to this project such as the team who built the original compressor cascade and the team who built the calibration tunnel.

> "I will praise thee; for I am fearfully and wonderfully made: marvellous are thy works; and that my soul knoweth right well." Ps 139:14

Contents

List of Figures

List of Tables

1 Introduction

Improving compressor performance is important to the overall efficiency of a jet engine. Compressors are of particular interest due to their contribution to the overall cost of gas turbines in both manufacturing and operational costs. They are one of the heavier components of the engine because of the large number of stages needed to achieve the necessary pressure ratios. Operational costs, such as costs of fuel burn and maintenance, can be reduced by decreasing engine weight and size. Therefore, much of the focus in compressor research is to decrease the overall costs using flow control. Flow control is one means of achieving greater engine efficiency by improving compressor aerodynamics. Flow control is used to reduce boundary layer separation on compressor blades. The cost of flow control is measured by the cycle cost and must be such that its application does not hinder engine performance.

1.1 Motivation

Flow control techniques have been studied in the application of gas turbine compressors by a number of researchers. Their work has shown that flow control can be used to delay boundary layer separation on the suction side of compressor blades. Boundary layer separation causes losses and are an important factor in compressor stall.

The methods that have been investigated include direct streamwise injection, steady/pulsed vortex generator jets, boundary layer suction, and plasma actuators. However, all have been studied as active control techniques which require the input of energy such as a source of high-pressure air or a voltage supply. In most of the cases described above, the requirement is high pressure air that must be bled from a downstream stage of the compressor, and supplied with sufficient mass flow to reattach the separated boundary layer on the flow controlled blades.

Passive flow control does not require energy input, but uses the pressure distribution generated by air flow over the blade profile. It does not require bleed air and therefore does not adversely affect the thermodynamic cycle of the engine in the way active flow control does. Vortex generator jets in passive flow control are driven by the pressure difference between the pressure and suction side. The air travels through

inlet holes on the pressure side into the plenum of the blade. After mixing in the plenum, air exits through jet holes on the suction side to mix with boundary layer.

Potential applications of passive flow control include propulsion gas turbines and land based power generation gas turbines. The research presented in this thesis is motivated by the potential savings in the applications of passive flow control in axial compressors in propulsion gas turbines.

The number of blade rows dictate the weight and ultimately the cost of an axial compressor. There is interest in decreasing number of blade rows while still achieving the same overall pressure rise across the compressor. In order to do this, each stage must have increased aerodynamic loading which must come from either increased rotational speed, or increased flow turning.[1] Material properties determines the maximum shaft speed, focusing this research on aerodynamic loading of each blade row.

The loss generated by a compressor blade can be divided into three categories, all of which are increased in highly loaded blades, if not properly controlled. These losses are Profile Loss, Secondary Loss, and Tip Clearance Loss. Profile loss is the primary loss mechanism caused by the shape of the blade and its boundary layer in an adverse pressure gradient. Secondary loss is caused by energy lost to three dimensional flow due to the pressure gradients existing normal to the flow direction in the passage between two blades, which are aggravated by endwall effects and non-

[1]Further explanation in Chapter 2.

uniform upstream conditions. Finally, tip clearance loss is caused by vortices that are formed by air leaking through the gap between rotor blades and their casing. While the reduction of all three loss mechanisms has been studied with active flow control techniques, this research focuses on minimizing profile losses with passive flow control. It uses the blade shape to generate pressure gradients that drive jets between the pressure and suction side of the blade.

Research of passive flow control is motivated as a means of achieving more efficient and less costly gas turbines. Previous research analyzed flow control techniques for increasing the operational range of gas turbines by reducing losses associated with aerofoils experiencing high incidence which occurs at off-design operating points. In this cascade analysis, highly loaded blades were designed to separate at zero incidence, i.e. simulating the design operating point, in order to study the use of passive flow control generate a loss reduction of the separated flow, yielding a loss equivalent to a conventionally loaded axial compressor.

1.2 Research Objective and Approach

The objective of the research presented in this thesis is to describe a technique to increase stage loading with highly loaded compressor blades. Passive flow control with vortex generator jets are used as a method to control profile losses. The objectives of

this research are to:

1. Commission the linear compressor cascade by varying tailboard angles and inlet bleed slot width
2. Measure surface pressure distribution on an instrumented blade
3. Measure velocity of vortex generator jets
4. Analyze effect of variation in jet inlet diameter
5. Measure the boundary layer thickness with/without flow control
6. Compare the effectiveness of passive/active flow control with measurements of profile loss

Experiments were performed on a seven blade linear compressor cascade to analyze the effectiveness of flow control with vortex generator jets on highly loaded blades.

2 | Background

2.1 Literature Review

2.1.1 Historical Perspective

For a long time, linear compressor cascades have been used to research aerodynamic parameters because of their ease in experimental setup compared to full test rigs. Wennerstrom(1990) provides a historical perspective on the early developments of cascade research, specifically in the area of flow control[23]. Several techniques are described to increase diffusion by boundary layer control to achieve the desired pressure rise. Flow control methods were originally derived from successful application of flow control on aircraft wings. One of the earliest applications of passive flow control was in the form of midspan slots which suggested good performance along the midspan section, but did not compensate for losses near the endwall. The slots

were expected to produce better results in low aspect ratio blades and lower Mach numbers.

Another technique was tandem airfoils which were practically full-span slot blades with connectors to maintain structural integrity. Tandem airfoils demonstrated similar results to blades with slots with no improvements in the operating range. Vortex generator tabs showed 1 to 2 percent efficiency increase when placed on outer casing of rotating compressor rigs. They slightly increased stall margin at design speed. Vortex generator tabs were found to be one of the most successful applications because although the improvements were small, they did not have negative contributions like slots.

Active control techniques such as suction and blowing were also studied with an objective to increase stall margin. Steady blowing on the compressor casing yielded negligible effects in stall margin throughout experiments with uniform inlet flow. With distorted inlet flow, the stall margin had a significant increase. Even with blowing turned off, the presence of the blowing holes produced increased stall margin with distorted inlet conditions. Suction had similar effects as blowing in uniform flow but demonstrated poorer performance when compared to blowing in distorted inlet flows. These results led to developments of compressor case treatments.

Greenblatt et al. (2000) provides another historical perspective of flow control by

excitation in gas turbines[10]. Boundary layer control has traditionally been executed by injection or suction. Generally, suction has not been implemented because of mechanical complexities and added weight, offsetting aerodynamic gains. Blowing can be achieved by both passive and active processes.

Passive blowing done by slots, which allow air to flow through the blade, yielded favorable improvements in boundary layer control. Active flow control is carried out with flow supplied by an auxiliary compressor or bleed flow. Typically, separation control is governed by momentum addition rather than mass. A momentum coefficient is necessary to compare different experiments with active flow control. Certain cases indicated detrimental effects for low momentum coefficient addition to the flow.

Acoustic excitation as a means of flow control was also described by Greenblatt et al. (2000). It required high levels of excitation and only proved to have positive effects with low Reynolds numbers. Finally, Reynolds Averaged Navier-Stokes(RANS) methods do not allow the proper characterization of the flow because of the mesh size differences and assumptions made during computation. Hecklau et al. (2010) discussed how RANS fail to predict complex flow phenomena involving active flow control[12]. Even doubling time steps and internal iterations per cycle did not improve results.

2.1.2 Current Developments

Nerger et al. (2011) studied tangential blowing on the suction side and endwalls to decrease suction side separation and secondary flows[18]. Vortex generator jets were used as momentum input to increase mixing between boundary layer and outer flow in highly loaded low pitch to chord ratio controlled diffusion compressor blades. A combination of both blowing methods yielded best results in reducing profile and secondary losses, and increased the static pressure by 8 %. Increasing the mass flow ratio above mj/mi = 1% produced little effect on flow performance indicating that there is a maximum theoretical improvement limit with flow control.

Heckalu et al.(2010) discussed how suppressing flow separation allows blade to withstand higher adverse pressure gradient[12]. Suction surface experiences three dimensional separation near the endwalls which significantly contributes to blockage. With a controlled diffusion blade, the suction peak is generally followed by a separation bubble with laminar-turbulent transition. Turbulent reattachment is denoted by an increasing pressure gradient and high pressure fluctuation. Pressure induced boundary layer separation occurs due to diffusion of the flow.

For low aspect ratios, corner stall has significant impact on total pressure loss and passage blockage. Heckalu et al.(2010) analyzed pulsed blowing out of sidewalls and blowing through actuators mounted on the suction surface. Suppressing boundary

layer separation resulted in a static pressure rise of 8% as well as 13% reduction in pressure loss.

Culley et al. (2005) described how active flow control had proven success in external flows[3] . With an objective to increase the range of incidence and aerodynamic loading, impulsive injection with 50% duty cycle at 500 Hz yielded the same results as steady injection with much less mass fraction.

Some of the benefits of AFC are that it can be switched off and adapted to different operational requirements such as take-off and landing. Gmelin et al. (2012) commented on how unsteady jets are the most studied actuation methods [9]. The researchers analyzed synthetic jets, which are zero net mass flux jets. They concluded that synthetic jets have a potential to reduce total pressure loss with small blowing angles. When compared to pulsed or steady jets, Gmelin et al. deduces that synthetic jets are less effective at separation control.

Finally, Nguyen et al. (2007) described an adaptive feedback control[19]. In previous experiments, AFC was analyzed with constant blowing parameters which were never adapted to downstream conditions as the experiment progressed. Nguyen et al. (2007) analyzed active flow control with adaptive feedback using one dimensional unsteady Euler equations of motion. The main parameter for the feedback control method was total pressure measured downstream.

2.1.3 Passive Flow Control Parameters

As described in Evans (2009), a jet in crossflow generates a counter-rotating vortex pair which re-energizes the boundary layer by drawing high momentum fluid from the outer boundary layer into the inner boundary layer[6]. Figure 2.1 shows a normal impinging jet and its trajectory. The jet may be pitched and skewed to the surface

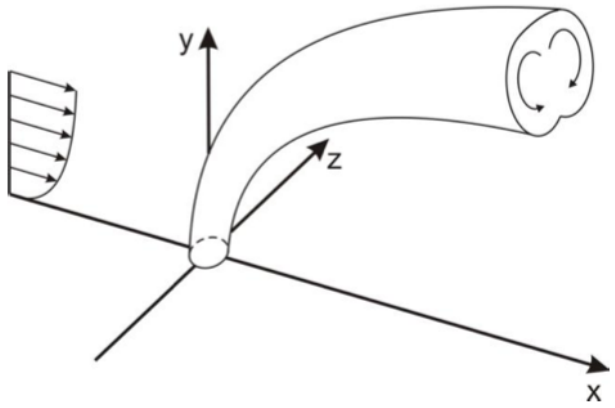

Figure 2.1: Normal Jet in Crossflow[6]

to disturb pressure field symmetry resulting in a stronger streamwise vortex. This stronger vortex engulfs the weaker which results in a jet with slower decay time and higher vorticity. The strength of the resulting vortex depends on several parameters including jet velocity, pitch/skew angle, jet hole size, jet location and jet spacing. Evans (2009) describes the result of several researchers concluding that jet velocities have the greatest effect on the local jet velocity ratio of approximately one. Higher

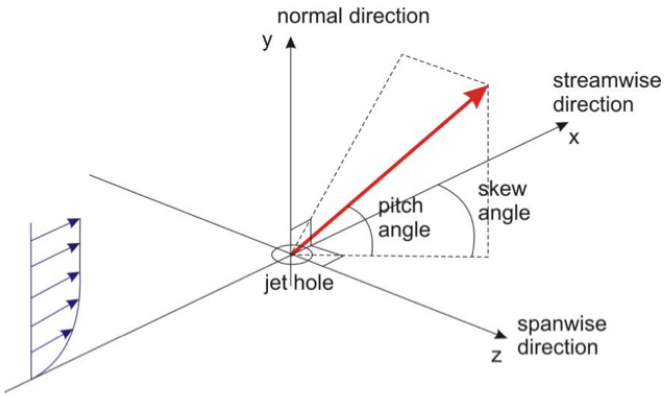

Figure 2.2: Skewed Jet in Crossflow[6]

velocities do not show any increased benefit in controlling separation in an adverse pressure gradient. In some cases, low velocity ratio actually increased boundary layer thickness and increased overall loss.

Jets were tested by several researchers over a range of skew angle between 0° and 90° resulting in maximum streamwise vorticity between 45° and 60°. Increasing pitch was found to increase jet penetration and streamwise vorticity. Jets pitched around 25° demonstrated highest levels of vorticity.

Jet hole size regulates mass flow rate and plays a crucial role in momentum addition of the jet. As the hole size increases for the same mass flow rate, velocity will decrease. Jet hole size was found to be most effective between one fifth and one half of the local boundary layer thickness. Finally, the jet location and spacing were most advantageous close to the separation location with a spacing between 9 and 12

diameters.

2.2 Cascade Aerodynamics

Since the flow field within a compressor is highly complex, simplified models are created to analyze the flow. The flow field is modeled as the sum of three two-dimensional flow fields, (a) Throughflow field, (b) cascade field (also known as blade-to-blade field) and (c) secondary flow field. The three dimensional coordinates of these flow fields are radial, r, circumferential, θ, and axial, z. In the through flow, the combined effect of all the blades in a row are considered rather than individual blades with coordinate system of (r,z). The cascade model performs flow analysis at each radius in a blade row or rather, in a meridional coordinate system (θ,s). The secondary flow model looks at the flow in (r,θ) plane analyzing the complex flow between the casing, hub, suction side and pressure side of a blade passage. For the purpose of this research the cascade view is used to analyze blade losses and the potential application of passive flow control.

2.2.1 Cascade Model

A linear compressor cascade is a two dimensional approximation of flow in a compressor. In a compressor, blades are evenly spaced around an annulus to form

a compressor row. Unwrapping a blade row into a linear form allows researchers to study parameters in the design of compressors. One of the main drawbacks of linear compressor cascades is that they do not accurately represent three dimensional effects present in rotating compressors. However, they are relatively cheap and easy to set up when compared to rotating compressor rigs.

The Euler equation relates how changes in fluid velocity induced by blade rows are related to thermodynamic changes across the machine. Consider the work interaction per unit mass flow rate that the streamtube undergoes in the meridional view. Assuming an adiabatic process, the energy equation becomes:

$$\frac{\dot{W}}{\dot{m}} = h_{t2} - h_{t1} \tag{2.1}$$

Work being done comes from the shaft in form of torque, therefore, $Pwr = \Omega T$, where Ω is the angular velocity and T is torque. Torque in the streamtube equals the rate of production of angular momentum as given by:

$$T = \dot{m} \left(r_2 v_2 - r_1 v_1 \right) \tag{2.2}$$

Now, equating the power input and $\dot{W}$ in gas flow results in:

$$\dot{W} = \dot{m}\left(h_{t2} - h_{t1}\right) = \Omega\dot{m}\left(r_2 v_2 - r_1 v_1\right) \tag{2.3}$$

The process of relating mechanical power and thermodynamics assumed steady and adiabatic flow. After simplification, the equation becomes:

$$h_{t2} - h_{t1} = \Omega\left[(rv)_2 - (rv)_1\right] \tag{2.4}$$

Ω or (rv) need to increase in order to obtain a higher stagnation enthalpy rise across the stage. Since upper limits of Ω are dictated by material properties, the difference in flow turning terms needs to increase. $\Delta(rv)$ dictates the need for highly loaded blades which can obtain the theoretical flow turning necessary. Increased flow turning is achieved by increasing the metal turning angle and keeping the flow attached using flow control.

2.3 Turbulence Intensity

In order to understand flow turbulence, statistical analysis is necessary. The local flow velocity vector is decomposed in three components u, v, w. Furthermore, the set

of $u(t)$ can be decomposed into its mean,$\bar{u}$ and turbulent fluctuation values,$u'(t)$.

$$u(t) = \bar{u} + u'(t) \tag{2.5}$$

The mean velocity and turbulent fluctuation are calculated from N discrete, equi-spaced points using:

$$\bar{u} = \frac{1}{N}\sum_{1}^{N} u_i \tag{2.6}$$

$$u_i' = u_i - \bar{u} \tag{2.7}$$

The turbulence strength is the root mean squared of the fluctuation velocity, i.e.:

$$u_{rms} = \sqrt{\frac{1}{N}\sum_{1}^{N}(u_i')^2} \tag{2.8}$$

Finally, the turbulence intensity is given by the turbulence strength divided by mean velocity.

$$I = \frac{u_{rms}}{\bar{u}} \tag{2.9}$$

Turbulence intensity is a measure of the size of fluctuations compared to the mean velocity. Larger turbulence intensity values indicate larger turbulence in the flow. Vortex generator jets increase turbulence in the boundary layer which delays boundary layer separation by mixing high velocity air outside of the boundary layer with flow

inside the boundary layer.

2.4 Vorticity

Vorticity is a measure of rotation in a fluid vector field. In mathematical terms, Vorticity, ξ, is equal to the curl of the velocity field.

$$\xi = \nabla \times \mathbf{V} \tag{2.10}$$

$$\xi = \left(\frac{\partial w}{\partial y} - \frac{\partial v}{\partial z}\right)\mathbf{i} + \left(\frac{\partial u}{\partial z} - \frac{\partial w}{\partial x}\right)\mathbf{j} + \left(\frac{\partial v}{\partial x} - \frac{\partial u}{\partial y}\right)\mathbf{k} \tag{2.11}$$

Secondary flow downstream of the cassette is a two-dimensional flow, transverse to the cassette flow, independent of streamwise components. In this case, vorticity becomes the following scalar field:

$$\zeta_{i,j} = \left(\frac{\partial v}{\partial x} - \frac{\partial u}{\partial y}\right)_{i,j} \approx \left(\frac{\Delta v}{\Delta x} - \frac{\Delta u}{\Delta y}\right)_{i,j} \tag{2.12}$$

A discrete approximation of the flow is obtained by probe traverses and finite difference is used to compute vorticity by:

$$\zeta_{i,j} = \frac{v_{i+1} - v_{i-1}}{2\Delta x} - \frac{u_{j+1} - u_{j-1}}{2\Delta y} \tag{2.13}$$

3 | Experimental Setup

3.1 Linear Compressor Cascade

The number of blades in a linear compressor cascade is dictated by cascade design and wind tunnel limitations. Wind tunnels have a prescribed exit area and maximum velocity they can achieve, both of which are taken into consideration during the design of the experiment in order to match desired Reynolds numbers inside a typical gas turbine compressor. Researchers have used anywhere from 3 to over 15 blades in linear compressor cascades[1].

Figure 3.1 shows the schematic of a linear compressor cascade. Seven identical blades are used to set up the experiment to obtain periodic flow. The four outermost blades are present to allow the middle three blades to achieve periodicity. A periodic flow is obtained when the three middle blades have similar flow characteristics such as peak profile loss and outflow angle. Two outflow tailboards and inlet bleed slots

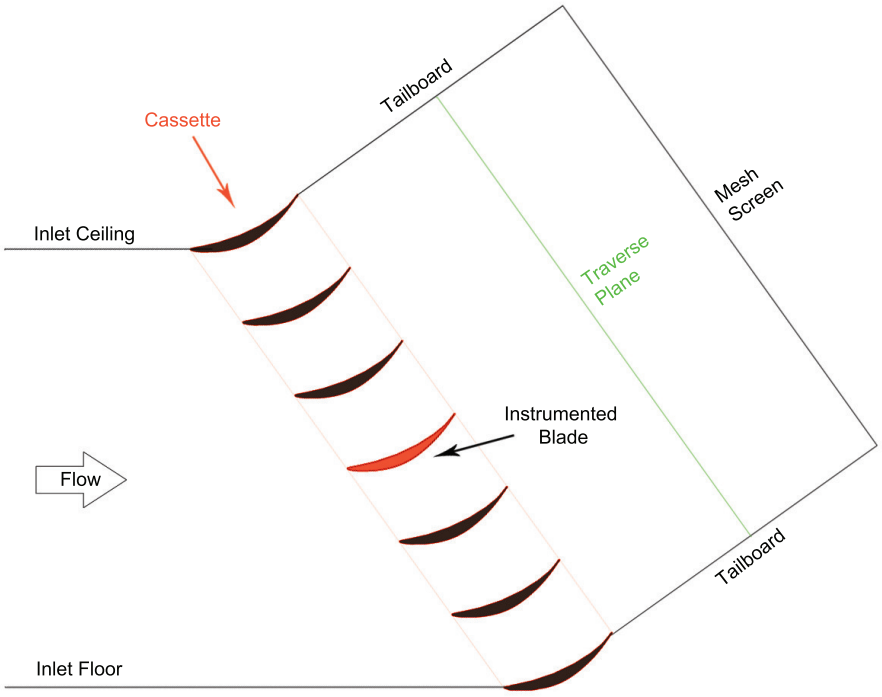

Figure 3.1: Schematic of a Linear Compressor Cascade

were designed to aid in obtaining a periodic flow. The middle blade is instrumented with pressure taps along the midspan. Once a periodic flow is achieved, data is obtained from the middle blade. A downstream traverse plane allows for pressure measurements downstream of the cassette(i.e. the portion of the cascade holding the blades themselves). The mesh screen pressurizes the cascade before the flow exits to atmospheric conditions.

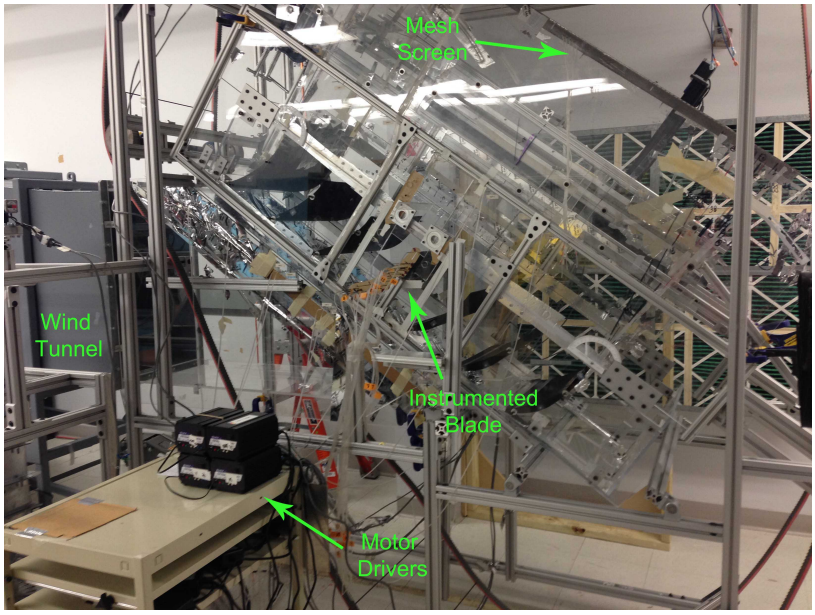

Figure 3.2: Linear Compressor Cascade at WPI

The WPI seven blade linear compressor cascade is shown in Figure 3.2. The compressor cascade has seven static pressure taps upstream and downstream of the cassette located at equal pitchwise positions in each passage. The upstream static pressure taps are used to measure the inlet pressure distribution. A five-hole probe traverse was used to measure total pressure, static pressure and both pitchwise and spanwise flow direction, one chord downstream of the cassette.

Reynolds Number	500 000
Blade Inlet Flow Angle	54.4°
Blade Outlet Flow Angle	0°
Solidity	1.35
Stagger Angle	27.3°

Table 3.1: Cascade Parameters

Table 3.1 provides a summary of the main parameters describing the cascade. The blades have an inlet flow angle of 54.4° and were designed to be tested at a Reynolds number typical of an early compressor cascade stage. Figure 3.3 shows a schematic of the cascade parameters. Solidity is defined as the chord divided by pitch.

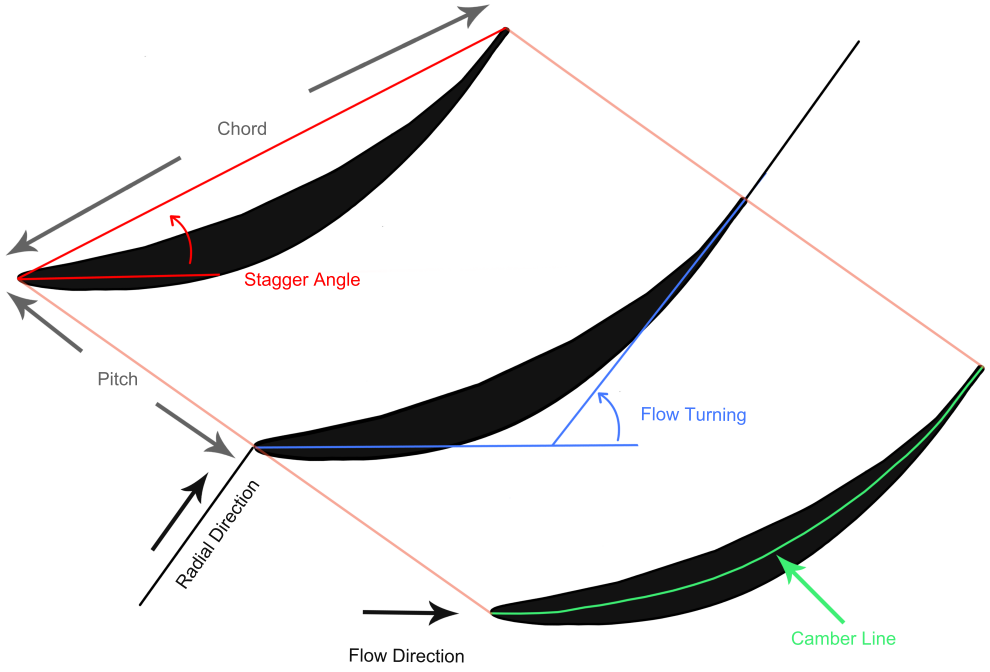

Figure 3.3: Cascade Definitions

The blade tested is a modified NACA 65 series blade with a refined camber distribution, moving the suction peak closer to the leading edge[16]. Figure 3.4 contains a

profile of the modified blade. A blade insert is shown which was designed to accommodate a blade plenum that drives the vortex generator jets. The endwall pegs were holes fitted to hold the blades and tip gap spacers.

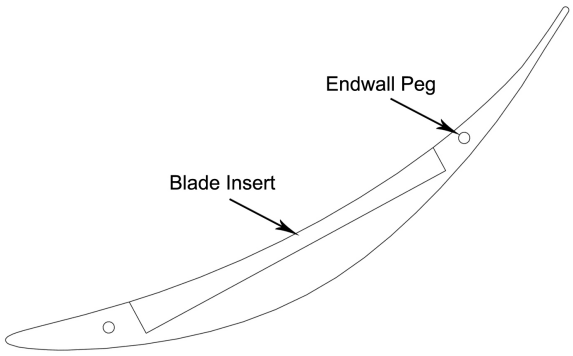

Figure 3.4: Profile of the Highly Loaded Blade

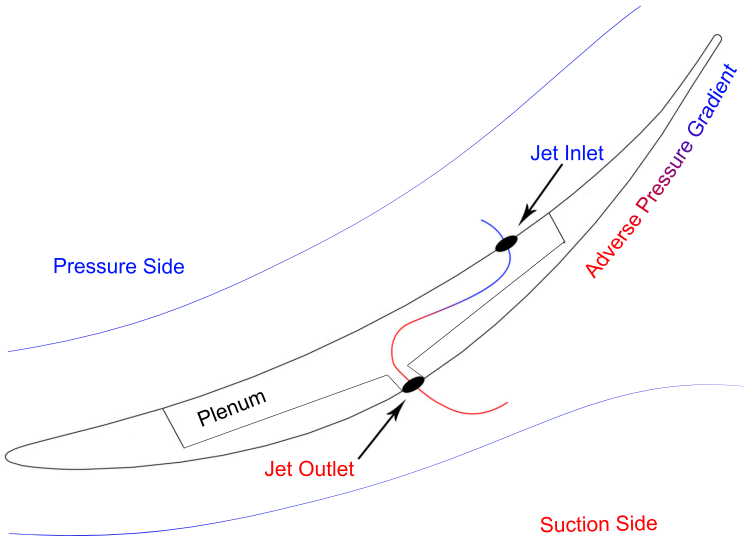

Figure 3.5: Midspan Profile of the Highly Loaded Blade

The midspan blade profile is shown in Figure 3.5. Holes on the pressure side allow for air to travel inside the blade where it mixes in the plenum. Since the pressure is lower on the suction side, pressurized air in the plenum is driven out of vortex generator jet holes on the suction side.

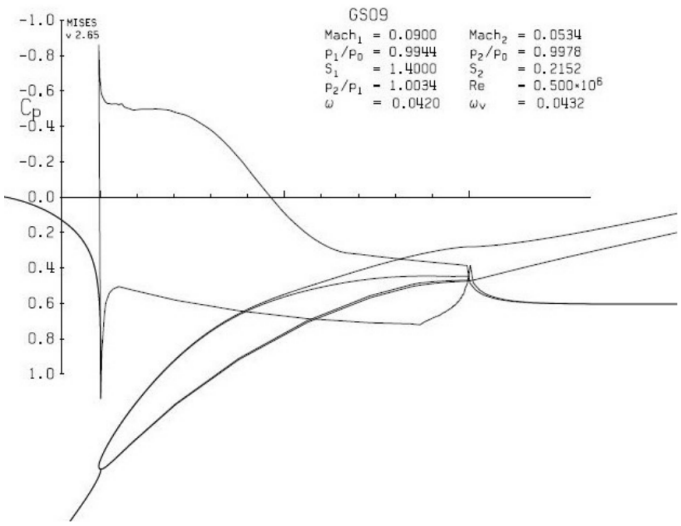

Figure 3.6: CFD Prediction of Pressure Distribution of Highly Loaded Blade With Flow Separation

Computational analysis of the blade was performed with MISES, a two dimensional Computational Fluid Dynamics(CFD) Euler code with a momentum integral boundary layer solver. The CFD analysis was executed with the same inlet conditions the blade would encounter in the compressor cascade. As described by Meyer et al. (2011), the pressure distribution of the blade indicated a boundary layer separation located approximately at 65% chord[16]. This is shown in Figure 3.6.

3.2 Calibration and Hardware

3.2.1 Calibration Tunnel

A calibration tunnel was designed and assembled by a MQP team at WPI to obtain precise and reliable calibration data of hotwire and 5-hole pressure probes[2]. High precision rotary tables ensured reliable positioning of the probe over a vast range. The range of the calibration tunnel probe manipulator allowed for calibration of hotwire anemometers parallel and perpendicular to the flow. Figure 3.7 shows the calibration tunnel.

In order to reduce vibrations while running the calibration tunnel, the feet were removed and replaced with 1.5" aluminum bars. Cross supports were attached to the two main cantilevered bars that hold the rotary mechanism. The supports were then attached to the cascade rig which greatly diminished probe vibration.

A motor controller was designed and built to power the DC motor at various speeds. Drivers were written to control the positioning of the probe using labVIEW. Matlab was used to process all the data.

Verification of the calibration tunnel was performed by traversing a five-hole probe over the exit of the calibration jet at different heights. As seen in Figure 3.8, the calibration tunnel exhibits constant outflow velocity over the measurement area. Fur-

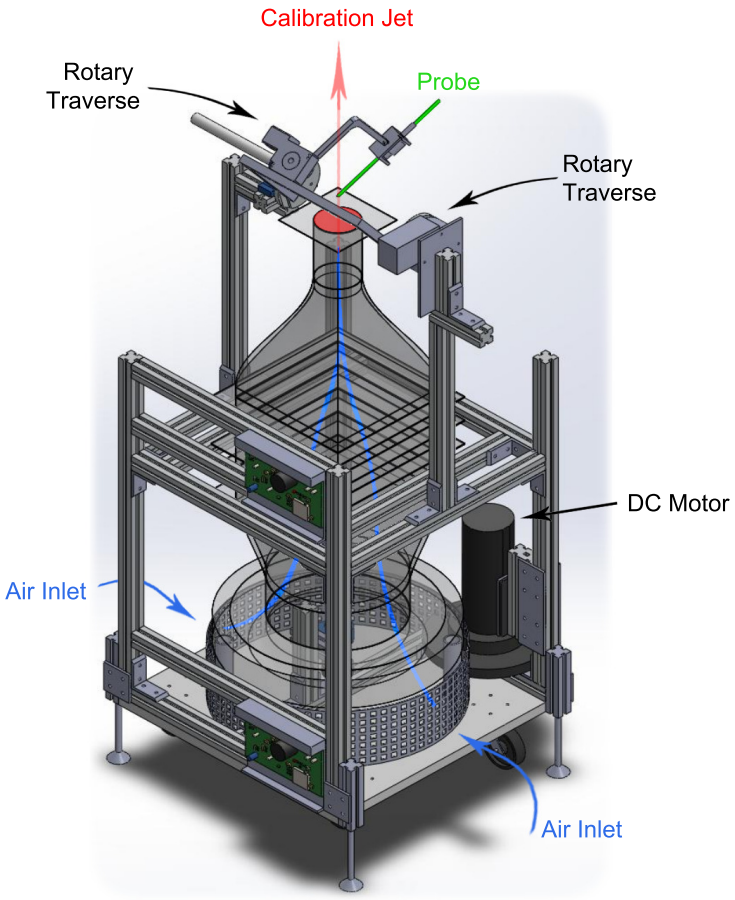

Figure 3.7: Velocity Probe Calibration Tunnel

thermore, the size of the highest velocity contour indicates that errors in alignment of the probe with the center of rotation would not generate errors with the calibration.

The probe manipulator is capable of achieving rotations in both pitch and yaw

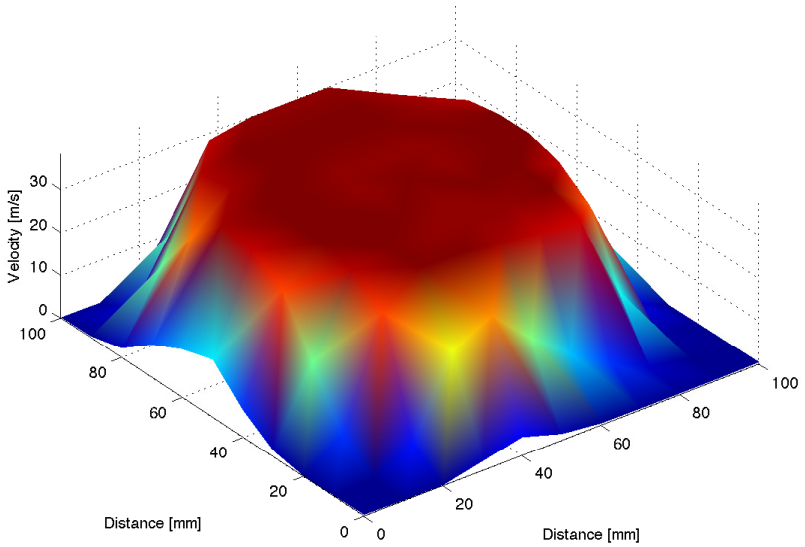

Figure 3.8: Calibration Tunnel Jet Velocity

while maintaining the probe tip at the center of the outlet area. The range varies from $-40°$ to $90°$ for pitch and $-40°$ to $70°$ for yaw. This calibration tunnel was used to calibrate the five-hole probe and various hotwire anemometers.

3.2.2 Pressure Measurement

Pressure measurement was performed through a Pressure Systems Inc NetScanner Model 9116, which is a 16 port differential pressure transducer. The PSI 9116 has a measuring accuracy of $\pm$ 0.1 % full-scale resulting in a measurement uncertainty of 1.03 [Pa].

Lab auxiliary pressure allowed for actuators in the instrument to open both sides

of transducer to atmospheric pressure to perform a re-zero calibration. A re-zero calibration obtains an offset which is added to all measurements which compensates for any changes in atmospheric conditions. A full span calibration was performed by the manufacturer prior to the beginning of these experiments.

The 9116 pressure transducer is limited by the acquisition rate of 400 samples per second. For this reason, the 9116 pressure transducer was only used for time averaged results. Data presented was acquired at 400 samples per second over 2 seconds and then averaged. Drivers were written in labVIEW to communicate with the PSI and acquire data at the precise location.

All of the pressure lines connected to the pressure transducers were of the same diameter Tygon tubbing. The pressure lines were cut at similar lengths to minimize differing acoustic effects between lines.

3.2.3 Five-Hole Probe

A United Censor DC-125 five-hole probe is used to measure static/stagnation pressure and flow angle. The arrangement of the hole can be seen in Figure 3.9. The middle hole measures stagnation pressure as it is oriented normal to the flow. The four other holes are oriented on planes 45° to the flow and are used to determine pitch and yaw. The average static pressure is given by averaging the outside ports, P_2 to

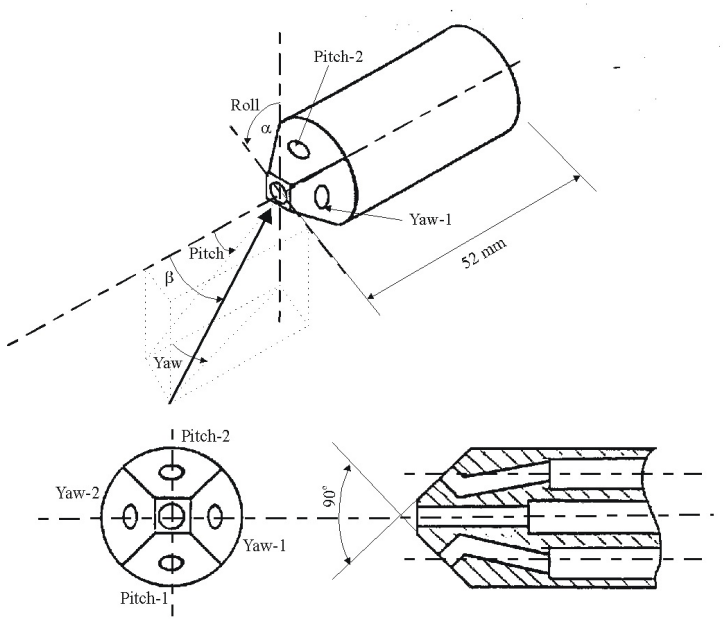

Figure 3.9: A Five Hole Probe Tip[1]

P_5. Pressure coefficients in both pitch, α, and yaw, β, are calculated by:

$$C_{P\alpha} = \frac{P_2 - P_3}{P_1 - P_{avg}} \tag{3.1}$$

$$C_{P\beta} = \frac{P_4 - P_5}{P_1 - P_{avg}} \tag{3.2}$$

The five-hole probe was rotated in the calibration tunnel to obtain pressure coefficients for every angle. A calibration curve fit was determined using the pressure coefficients. The five-hole probe is used to obtain a loss profile coefficient by traversing the probe downstream of the cassette. A profile loss coefficient, Y_p, is calculated by subtracting

the stagnation pressure downstream of the cassette from the upstream stagnation pressure and nondimensionalizing by the upstream dynamic head.

$$Y_p = \frac{P_{01} - P_{02}}{P_{01} - P_1} \tag{3.3}$$

where P_{01} is upstream stagnation pressure, P_{02} is downstream stagnation pressure and P_1 is the upstream static pressure. Velocity is calculated by:

$$V = \sqrt{\frac{2\Delta P}{\rho}} \tag{3.4}$$

In order to check if the static pressure is the equivalent of a pitot static probe, the five-hole probe was placed in a suction-type wind tunnel with known static and stagnation conditions. Figure 3.10 shows the probe velocity and pitot static calculated velocity with the maximum error occurring at slower velocities. The error in the measurement is given by:

$$\%Error = \frac{V_t - V_p}{V_t} \tag{3.5}$$

where, V_t is the actual velocity and V_p is the measured probe velocity.

$$V = cV_p \tag{3.6}$$

A probe specific correction factor, c, was determined to be 0.9507. With this correction, velocities above 12 [m/s] have less than 1% error which encompasses most of the velocity measured in the experiments.

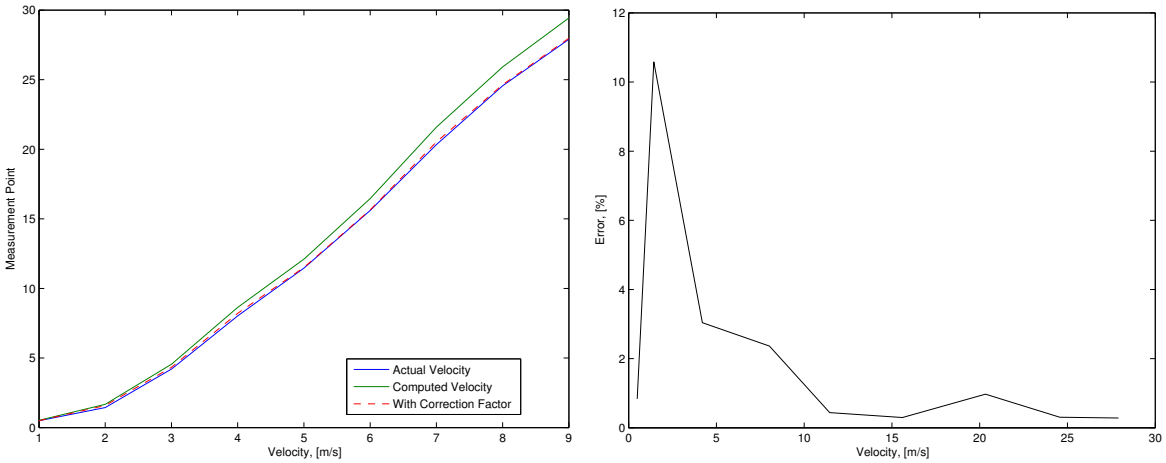

Figure 3.10: (a) Probe Velocity Comparison (b) Velocity Percent Error

3.3 Hot-Wire Anemometer

A hotwire anemometer is a thin wire probe used for measuring flow parameters. The hotwire is a constant-temperature anemometer which correlates changes in convection over a thin wire to flow velocity. A signal conditioner maintains a constant temperature by varying the current flow through the hotwire. Changes in required current are measured by a high sampling rate analog to digital converter. Figure 3.11 shows a miniature hotwire probe which was used to measure jet velocity.

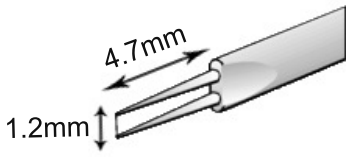

Figure 3.11: Miniature Hotwire Probe Used for Jet Velocity Measurement (Adapted From [5])

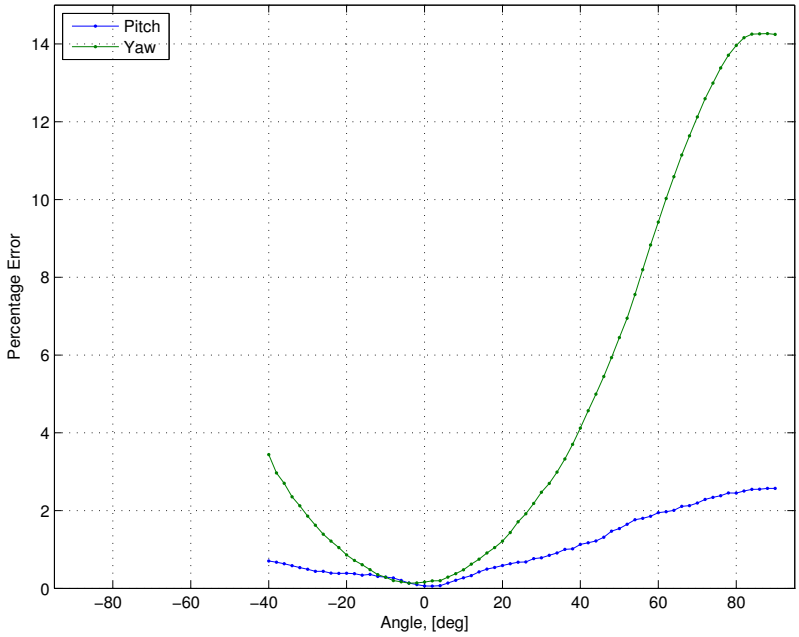

Figure 3.12: Hotwire Probe Validation

The miniature Dantec Dynamics 55P11 hotwire was used to measure jet velocity on the suction side of the blade. The jet hole diameter is 4.75[mm].The calibration tunnel was used to verify the probe's sensitivity with errors in positioning. Figure 3.12 shows the percentage error as a function of variations in pitch and yaw when

compared a probe. This experiment indicated that the probe experiences less than 2% error for variations in pitch and yaw less than 20°.

Hotwire anemometers are most sensitive to changes in temperature. Since running the wind tunnel for long periods of time increases the room temperature, a calibration was done before and after each experiment. Changes in calibration parameters were accounted for based on room temperature by linear interpolation between calibration curves which assume a linear temperature distribution between calibrations.

3.4 Traverse System

The linear compressor cascade was designed with two traverse systems, one for downstream measurement and one for tailboard positioning. In order to limit human errors in comparing various tailboard settings, a computerized traverse system allowed for accurate positioning of the tailboard angle. All of the traverse systems were motorized Velmex bi-slide systems which are accurate to 0.1 [mm].

3.5 Experimental Procedure

A probe holder was designed to support five-hole and hotwire probes. This probe holder allowed for traverses at varying angles from 50% chord length to anywhere

downstream of the flow. Several designs of the probe holder were tested and the probe holder that exhibited the least vibration and least flow disturbance was used for the experiments.

LabVIEW was used to perform calibration of the PSI and to home all the traverse systems prior to each experiment. For experiments with hotwire anemometers, a calibration was performed prior to each experiment and after. Atmospheric conditions were recorded with digital instruments and added to a database of experiment meta data. Finally, all the data was post-processed using Matlab.

3.6 Measurement Uncertainty

Uncertainly analysis was performed using the root mean squared deviation method. The uncertainty in velocity then becomes:

$$\delta V = \sqrt{\left(\frac{\partial V}{\partial \Delta P}\delta \Delta P\right)^2 + \left(\frac{\partial V}{\partial \rho}\delta \rho\right)^2} \tag{3.7}$$

Applying this method to the pressure coefficient in pitch yields the following equation:

$$\delta C_{p\alpha} = \sqrt{\left(\frac{\partial C_{p\alpha}}{\partial P_1}\delta P_1\right)^2 + \left(\frac{\partial C_{p\alpha}}{\partial P_2}\delta P_2\right)^2 + \left(\frac{\partial C_{p\alpha}}{\partial P_3}\delta P_3\right)^2 + \left(\frac{\partial C_{p\alpha}}{\partial P_{avg}}\delta P_{avg}\right)^2} \tag{3.8}$$

which results in an uncertainty of 0.22 [deg] for angles measured with the five-hole probe. Similarly for the profile loss coefficient, the uncertainty becomes:

$$\delta Y_p = \sqrt{\sum_{i=1}^{n} \left(\frac{\partial Y_p}{\partial P_i} \delta P_i \right)^2} \tag{3.9}$$

Table 3.2 provides a summary of measurement uncertainly for all the experimental data.

Pressure	± 1.03 [Pa]
Angle	± 0.22 [deg]
Velocity	± 0.12 [m/s]
Normalized Velocity	± 0.008
Profile Loss Coefficient	± 0.01
Turbulence Intensity	± 0.007
Hotwire Velocity[5]	± 1%

Table 3.2: Measurement Uncertainty

4 | Results

4.1 Commissioning

The aim of the commissioning process was to achieve a periodic flow in the cascade. The process of commissioning the linear compressor cascade involved traversing a five-hole probe downstream of the entire cascade. The main parameters varied to obtain a periodic flow were tailboard angle and upstream bleed slot size. In order to achieve a commissioned cascade, a range of tailboard angles were tested and the most uniform profile loss was chosen as the condition in which all the experiments were to be performed. Figure 4.1 shows the loss profile of the cascade prior to and after commissioning. The uncommissioned cascade features irregular loss profiles which indicate a non-uniform upstream flow condition as well as errors in incidence. The commissioned cascade features similar loss peaks for each of the three center blades as well as comparable wake sizes.

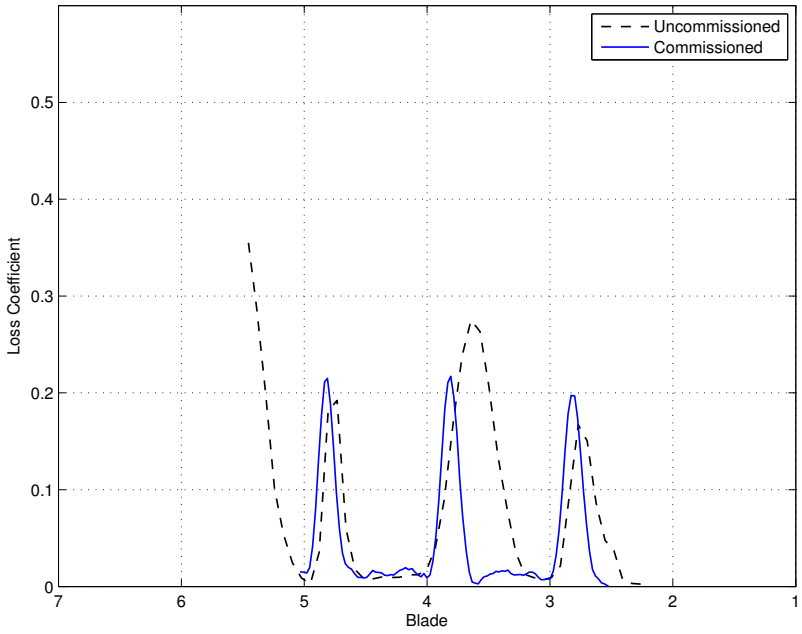

Figure 4.1: Commissioning of Compressor Cascade - Profile Loss

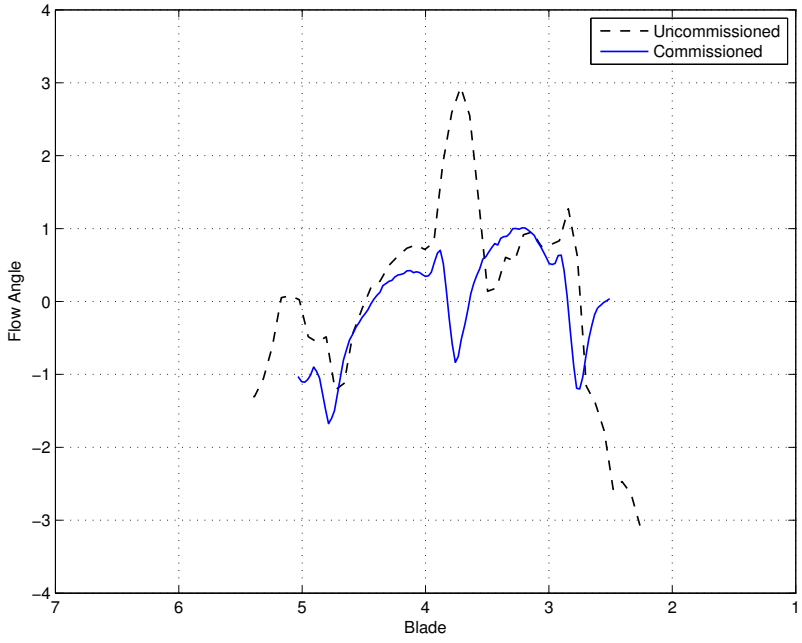

Figure 4.2: Commissioning of Compressor Cascade - Outflow Angle

Outflow angle is much more difficult to match and is differentiated by its positive peak followed by a negative peak. The middle of the two peaks coincides with the peak of the loss profile. Figure 4.2 indicates a good correlation in outflow angle between blades three and four following commissioning.

An area traverse was performed one chord downstream of the compressor cassette. Figure 4.3 shows the profile loss across the whole span of the instrumented blade. Two

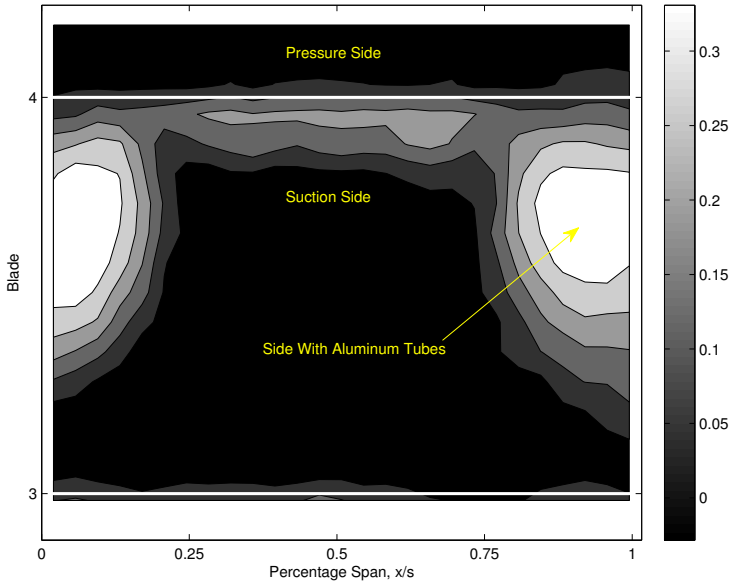

Figure 4.3: Area Traverse - Profile Loss

loss peaks are located at the ends of the blade with similar amplitude. These peaks are formed as a result of endwall corner separations interacting with tip gap flows. Although these peaks have the same magnitude, the peak on the right has a slightly

greater footprint than the left even though both tip gaps are the same width. A corner separation would create a clockwise vortex on the left and a counterclockwise vortex on the right while a tip leakage flow would do the reverse. As seen in Figure 4.4, the passage is dominated by corner separations. The presence of the tubes on the right reduces the leakage flow, which reduces its impending effect on the corner separation resulting in the bigger corner separation. Contours of vorticity indicate

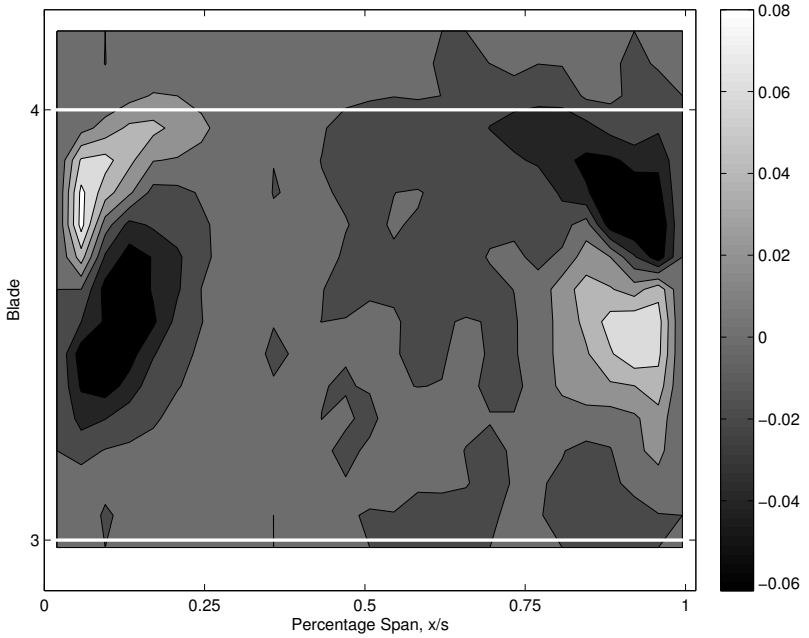

Figure 4.4: Area Traverse - Vorticity [1/s]

that the increased secondary flow interacts with the boundary layer up to one third of the span. These results confirm that the midspan traverses are not affected by the tip gap vortices if traversed at half span.

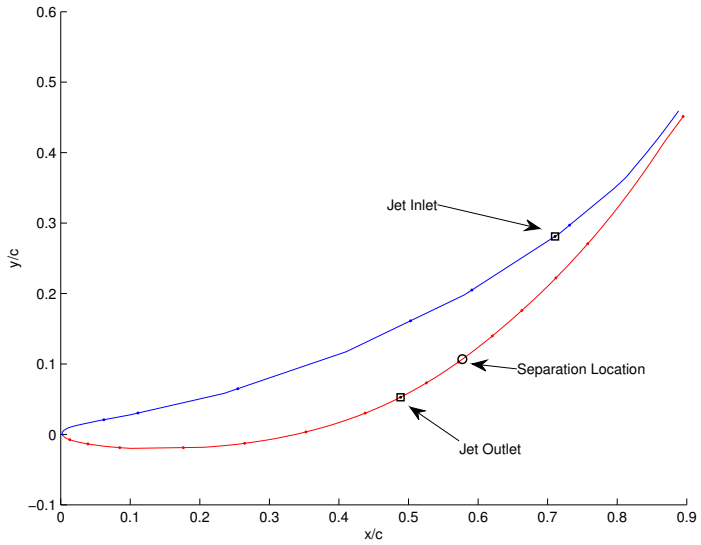

Figure 4.5: Blade Surface Pressure Measurement Locations

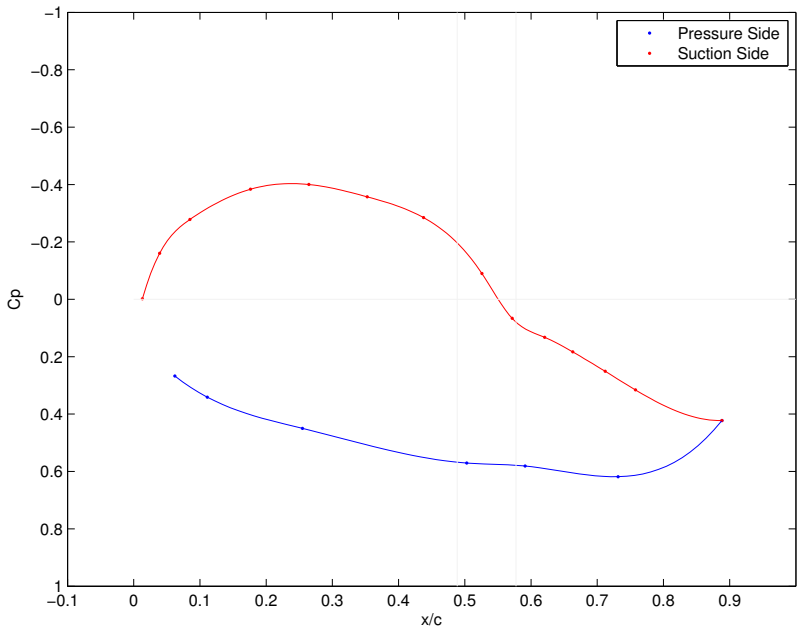

Figure 4.6: Blade Surface Pressure Distribution

Figure 4.6 shows the surface pressure distribution as measured by twenty static pressure tappings on the midspan profile. A profile of the blade denotes the location of each pressure measurement. The theoretical separation location calculated from computational results is also shown. This blade features a suction peak near 25% chord followed by diffusion of the suction side flow.

4.2 Boundary Layer Trip

The blade surface pressure distribution of the commissioned case does not indicate a full separation at the expected location. The flow over the blade appears to diffuse slowly and remain partially attached as is indicated by a pressure distribution that decreases from the suction peak to the trailing edge. In order to properly measure the effectiveness of flow control, a boundary layer trip was added near to the leading edge of the blade. The boundary layer trip is a thin aluminum wire with a diameter of 0.43 mm. Figure 4.7 shows the effect of the boundary layer trip. The suction peak moves slightly closer to the leading edge and is followed by a sharper decrease in velocity. As the velocity decreases, it achieves a maximum diffusion and then the boundary layer detaches from the suction surface as is indicated by the constant pressure from 60% chord to the trailing edge. With the boundary layer trip, the separation location matches numerical results.

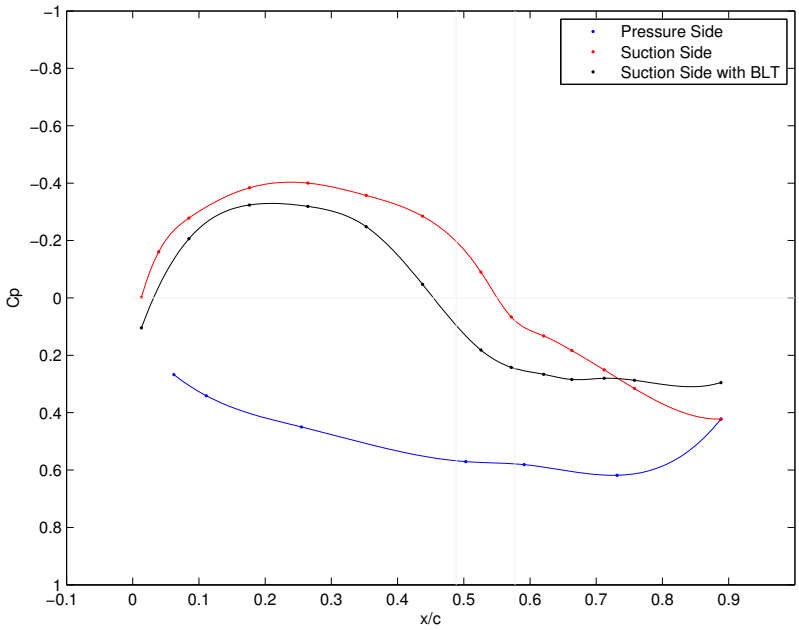

Figure 4.7: Blade Surface Pressure Distribution With Boundary Layer Trip

4.3 Flow Control

This section presents results on both active and passive flow control when applied to a highly loaded blade with significant suction side separation.

A hotwire inside the vortex generator jet hole is assumed to be measuring an average velocity with the plug flow model. Plug flow assumes a constant velocity across the circular cross section. Due to limitations of the probe holder mechanism for measuring the jet flow, a traverse across the jet was not performed and therefore, an averaged value measured in the center of the jet is presented.

4.3.1 Active Flow Control

Active flow control is achieved by closing the passive flow control inlet holes with tape and pressurizing the blade plenum. Pressure is supplied by lab pressure and is varied to obtain a range of jet velocities.

Active flow control results validate previous research on active flow control and its application for re-energizing a separated boundary layer. As is described in section 2.1.2, increasing the jet velocity ratio above one does not increase the effectiveness of controlling a separated flow. For the subsequent figures, active flow control is presented with a velocity ratio of 0.9.

4.3.2 Passive Flow Control

Jet inlet size diameter was varied between 3 mm and 7 mm. The variation in jet inlet size yields negligible change in jet velocity indicating that this particular design of passive flow control is not sensitive to jet inlet size. Furthermore, variations in tailboard angle did not significantly impact the jet velocity. Over the entire range tested, the maximum change in jet velocity ratio is 0.05. For subsequent figures, passive flow control is presented with a velocity ratio of 0.525 and a jet inlet diameter of 7 mm.

Figure 4.8 presents the boundary layer measured 30 mm downstream of the sepa-

ration location. The case without flow control, NFC, shows a typical boundary layer with adverse pressure gradient. Close to the surface of the blade, the velocity remains relatively constant up to 12 mm indicating a separated boundary layer. As the distance above the surface increases, velocity increases sharply over a range of 20 mm.

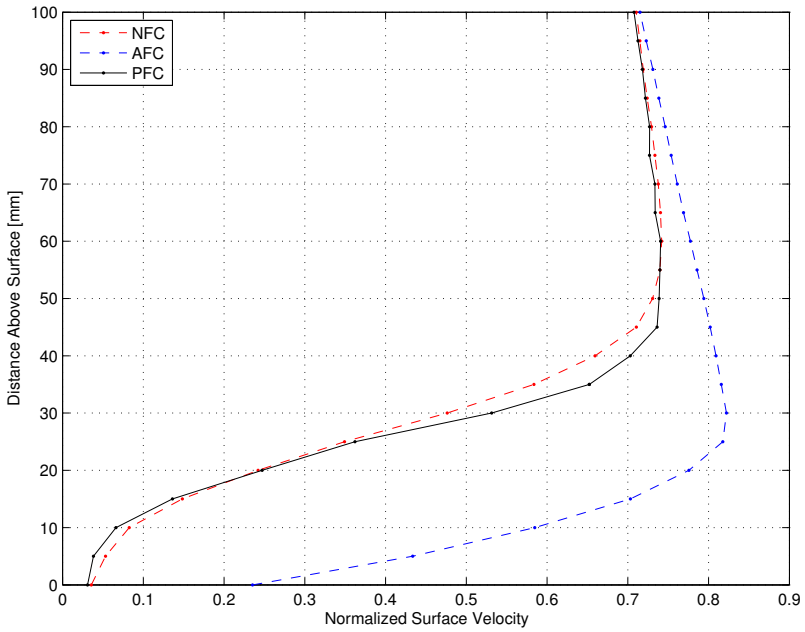

Figure 4.8: Comparison of Boundary Layer Velocity

Active flow control, AFC, has the greatest effect on the boundary layer. Close to the surface of the blade, the velocity ratio greatly increases as a result of the momentum addition. This indicates a full interaction and mixing of the boundary layer causing the flow to reattach. From the surface of the blade, a 20 % increase in

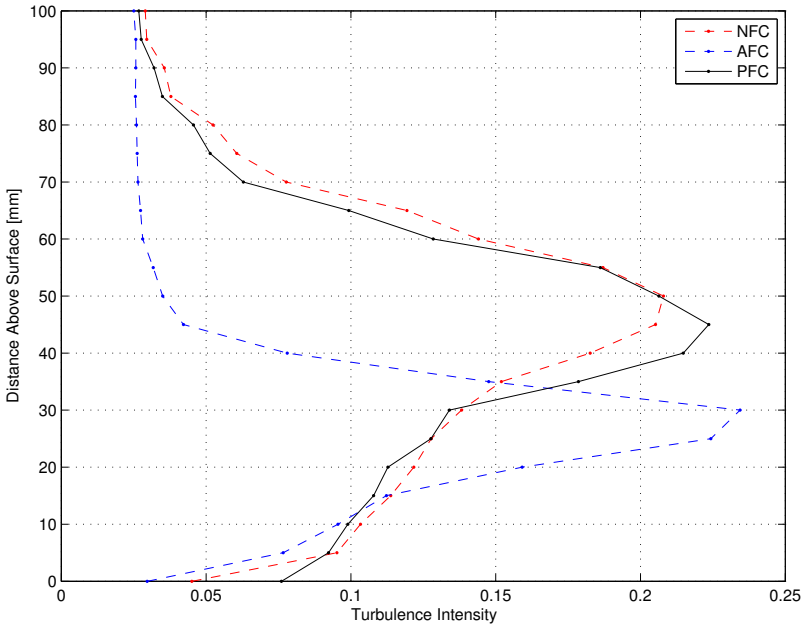

Figure 4.9: Comparison of Boundary Layer Turbulence Intensity

local velocity is seen. The boundary layer thickness decreased by 54 %.

Passive flow control, PFC, does not produce the reattachment of the separation that active flow control does because of the small jet velocity ratio. However, some effects are noticeable. Near the surface of the blade, the flow velocity appears greater than the case with no flow control. Overall, the boundary layer thickness is decreased by approximately 10% by the passive flow control.

Figure 4.9 shows the turbulence intensity of the boundary layer. Vortex generator jets increase the local turbulence levels both for active and passive cases. Active flow control features higher turbulence intensity close to the surface when compared to

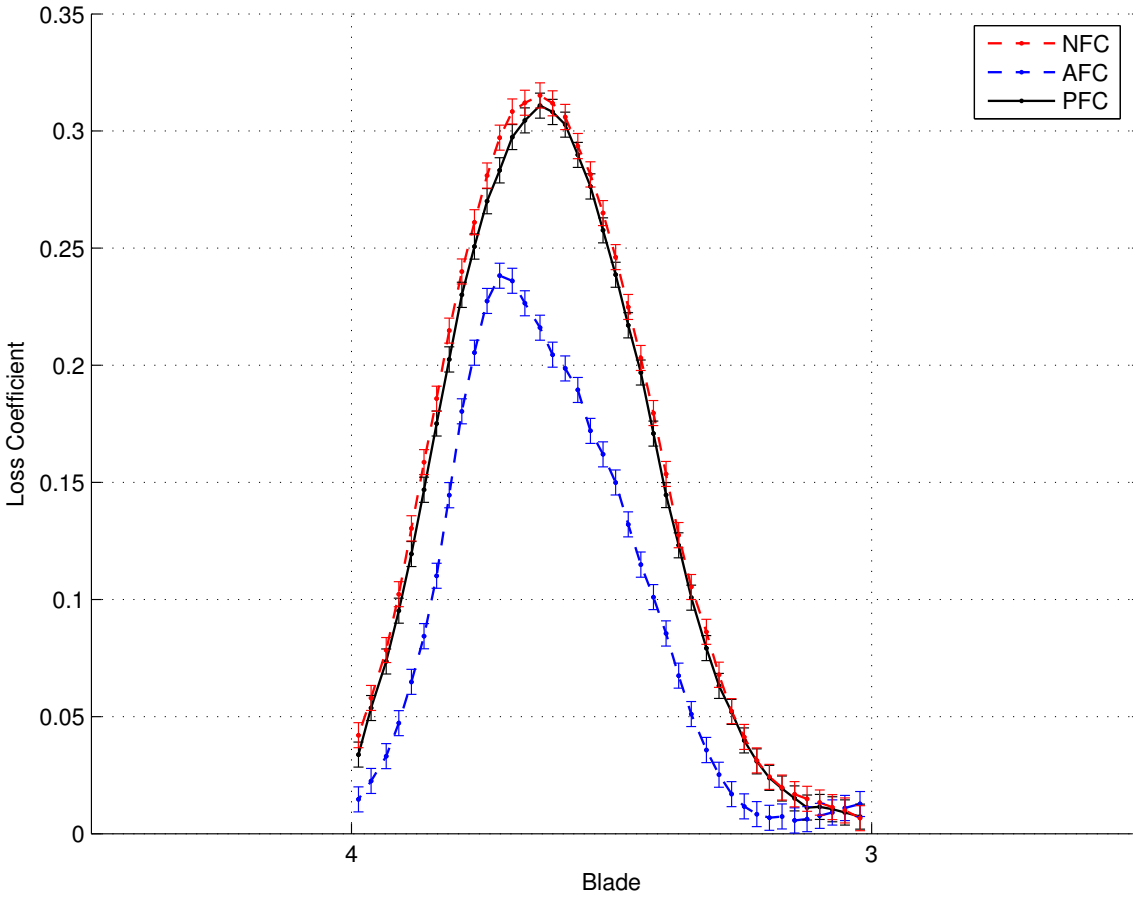

Figure 4.10: Comparison of Profile Loss

passive flow control. Comparing passive flow control and no flow control, passive flow control has a higher turbulence intensity. Finally, the overall profile loss of the blade with and without flow control is shown in Figure 4.10. Active flow control results in approximately 36 % decrease in the loss profile and passive flow control has reduction of approximately 4 %. However, as is indicated by the error bars, the uncertainty range in the passive flow control case encompasses the no flow control case making

the effect of passive flow control inconclusive at the achieved velocity ratio.

4.4 Spanwise Loss Profile

A spanwise area traverse normal to the surface in the same location as previous boundary layer traverses is shown in Figure 4.11. Without flow control, high losses near the surface show the separated flow.

The profile loss of the same area traverse with active flow control is shown in Figure 4.12. A significant reduction across the whole area is observed. The overall maximum in profile loss is not diminished but rather compacted closer to the blade surface. Figure 4.14 shows the difference in loss profile between the no flow control case and passive flow control. This indicates that the effect of passive flow control discussed in the previous section encompasses the whole midspan region of the blade.

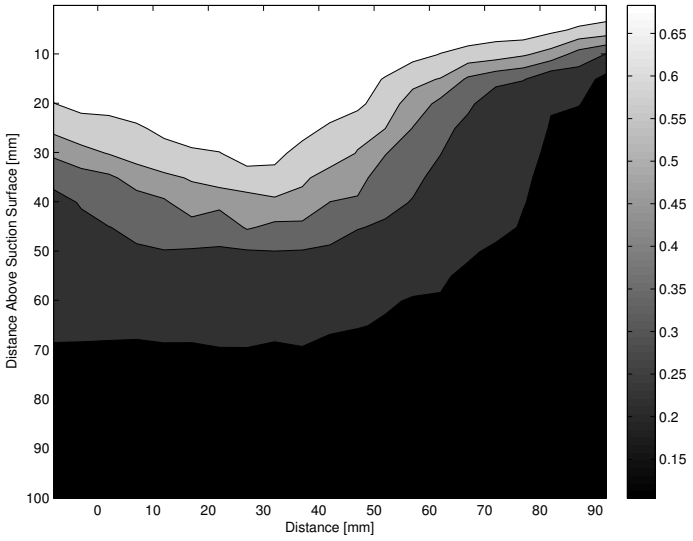

Figure 4.11: NFC Spanwise Traverse - Profile Loss Coefficient

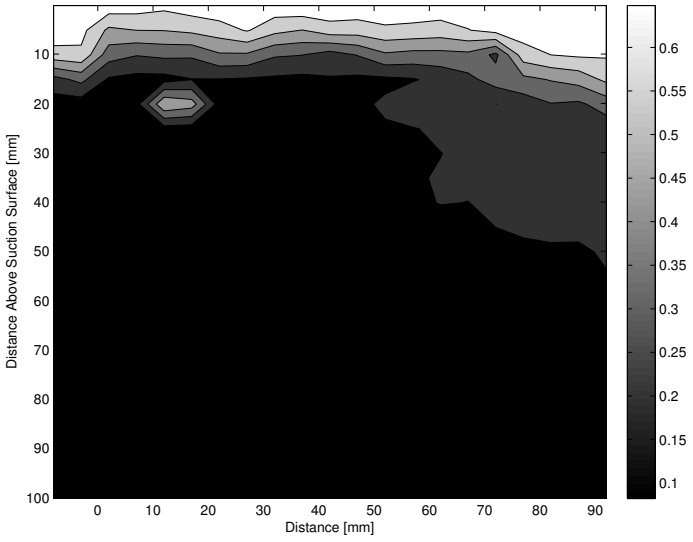

Figure 4.12: AFC Spanwise Traverse - Profile Loss Coefficient

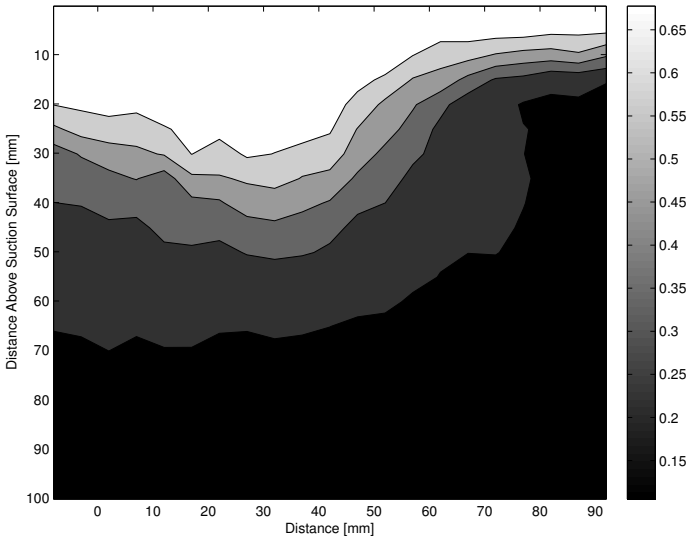

Figure 4.13: PFC Spanwise Traverse - Profile Loss Coefficient

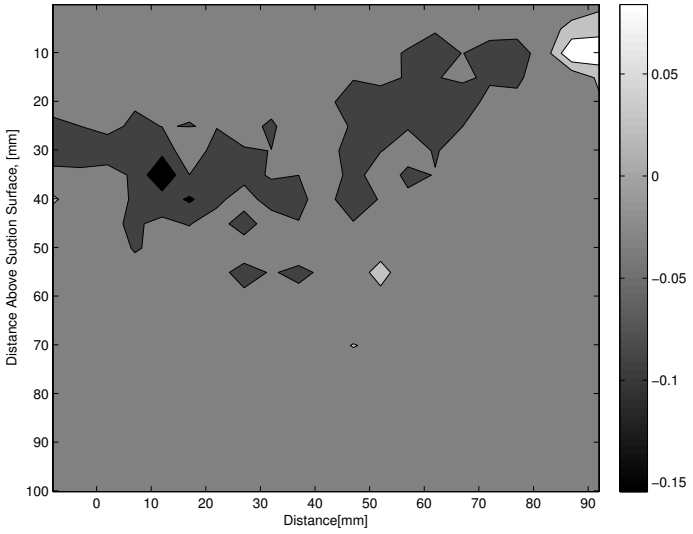

Figure 4.14: Spanwise Traverse - Difference in Profile Loss Coefficient

5 | Conclusions

A flow control method for minimizing losses in a highly loaded compressor blade was analyzed. Passive and active flow control experiments were conducted to demonstrate the potential application of passive flow control. The vortex generator jet velocity in the passive flow control was limited by the pressure difference across the blade, which was used to drive the jets.

Active flow control with a jet velocity ratio of 0.9 was found to be effective at controlling the separation and reducing midspan loss by approximately 37 %. Passive flow control, with a jet velocity ratio of 0.525 was found to have a negligible effect on the profile loss coefficient, and was not able to reattach the separated boundary layer. The success of active flow control with a velocity ratio of 0.9 suggests, that despite little effect of passive flow control, there is potential for passive flow control to be effective.

Similar results to active flow control can be achieved if the blade profile can be

optimized in such a way as to allow the generation of a higher velocity ratio jet. The blade used was not optimized but indicated benefits in loss reduction by flow control. In order to obtain higher jet velocity in passive flow control, the blade profile needs to be optimized to increase the jet velocity by maximizing the pressure difference between pressure and suction side near the jet location.

5.1 Future Work

One of the important sectors which this research can be applied is land based gas turbines for power generation. The working passive flow control parameters can be implemented in a variable incidence compressor cascade. The goal of this research would be to employ passive flow control to increase the operating range of land based gas turbines therefore increasing compressor efficiency performance during off-design operating conditions.

One of the big concerns of the implementation of passive flow control is the cost of manufacturing small channels and holes for the jets. Recently, NASA used 3D printing additive manufacturing to produce a combustor that is cheaper to manufacture and requires less time than conventional approaches[17]. Future work should take into consideration printed blades that feature built in channels for airflow.

Bibliography

[1] Joao Baiense, Francisca Chichester, Michael Egan, Steven Madamba, Sasha Moore, and Juliana Wakeman. Design of a moving bar wake generator for a linear compressor cascade. *Major Qualifying Project, Worcester Polytechnic Institute*, E-project-042612-030134, 2012.

[2] Paul Ciolek, Ethan Deragon, Daniel Frodell, and Stephen Kressaty. Design and construction of a velocity probe calibration rig. *Major Qualifying Project, Worcester Polytechnic Institute*, E-project-031113-224537, 2013.

[3] Dennis Culley, Edward Braunscheidel, and Michelle Bright. Impulsive injection for compressor stator separation control. In *Tech. Rep. NASA TM-2005-213859, NASA Glenn Research Center*, pages 1–10, Cleveland, Ohio, 2003.

[4] Diego H De La Riva, William J Devenport, Chittiappa Muthanna, and Stewart A L Glegg. Behavior of Turbulence Flowing Through a Compressor Cascade. *AIAA Journal*, 42(7):1302–1313, 2004.

[5] Dantec Dynamics. Probes for hotwire anemometer. `http://www.dantecdynamics.com/docs/support-and-download/research-and-education/probepost.pdf`.

[6] Simon Evans. *Flow Control in Compressors*. PhD thesis, University of Cambridge, 2009.

[7] Simon Evans, John Coull, Ibraheem Haneef, and Howard Hodson. Minimizing the Loss Produced by a Turbulent Separation Using Vortex Generator Jets. *AIAA Journal*, 50(4):778–787, 2012.

[8] Simon Evans, Howard Hodson, Tom Hynes, and Christian Wakelam. Flow control in a compressor cascade at high incidence. *Journal of Propulsion and Power*, 26(4):828–836, 2010.

[9] Christoph Gmelin, Vincent Zander, Martin Hecklau, Frank Thiele, Wolfgang Nitsche, Andre Huppertz, and Marius Swoboda. Active flow control concepts on a highly loaded subsonic compressor cascade: Resume of experimental and numerical results. *Journal of Turbomachinery*, 134(6):1–9, 2012.

[10] David Greenblatt and Israel J. Wygnanski. The Control of Flow Separation by Periodic Excitation. *Progress in Aerospace Sciences*, 36(7):487 – 545, 2000.

[11] M Hecklau, O Wiederhold, V Zander, R King, W Nitsche, A Huppertz, and M Swoboda. Active separation control with pulsed jets in a critically loaded compressor cascade. *AIAA Journal*, 49(8):1729–1739, 2011.

[12] Martin Hecklau, Vincent Zander, Inken Peltzer, Wolfgang Nitsche, Andre Huppertz, and Marius Swoboda. Experimental afc approaches on a highly loaded compressor cascade. In *Active Flow Control II*, volume 108 of *Notes on Numerical Fluid Mechanics and Multidisciplinary Design*, pages 171–186. Springer Berlin Heidelberg, 2010.

[13] J D Hughes and G J Walker. Natural transition phenomena on an axial compressor blade. *Journal of Turbomachinery*, 123(2):392–401, 2000.

[14] M Lemke, C Gmelin, and F Thiele. Simulations of a compressor cascade with steady secondary flow suction. In *New Results in Numerical and Experimental Fluid Mechanics VIII*, volume 121, pages 549–556. 2013.

[15] Liu Luxin, Yedidia Neumeier, and J V R Prasad. Active flow control for enhanced compressor performance. In *AIAA paper-4017. 41st AIAA/ASME/ SAE/ASEE Joint Propulsion Conference Exhibition*, Tucson Convention Center, Arizona, 2005.

[16] Alexander Meyer-Lorentson, Bridget Stevens, and Lane Thornton. Passive flow control in a highly-loaded compressor cascade. *Major Qualifying Project, Worcester Polytechnic Institute*, E-project-031411-141757, 2011.

[17] NASA. Industry test '3d printed' rocket engine injector. `http://www.nasa.gov/content/nasa-industry-test-3d-printed-rocket-engine-injector/#.U62z3Y1dVFE`.

[18] Daniel Nerger, Horst Saathoff, Rolf Radespiel, Volker Gummer, and Carsten Clemen. Experimental investigation of endwall and suction side blowing in a highly loaded compressor stator cascade. *Journal of Turbomachinery*, 134(2):1–12, 2011.

[19] Nhan Nguyen, Michelle Bright, and Dennis Culley. Adaptive feedback optimal control of flow separation on stators by air injection. *AIAA Journal*, 45(6):1393–1405, 2007.

[20] A Rona and H Soueid. Boundary layer trips for low reynolds number wind tunnel tests. In *48th AIAA Aerospace Sciences Meeting Including the New Horizons Forum and Aerospace Exposition*, pages 1–13, Orlando, Florida, 2010.

[21] Qing Tian, Roger L Simpson, and Genglin Tang. Flow visualization on the linear compressor cascade endwall using oil flows and laser doppler anemometry. *Measurement Science and Technology*, 15(9):1910–1916, 2004.

[22] Sumeet Trehan, Jaskirat S Sodhi, and Bhaskar Roy. Cascade studies of tandem blades for axial flow compressors/fans. In *44th AIAA/ASME/SAE/ASEE Joint Propulsion Conference Exhibit*, pages 1–11, 2008.

[23] A. J. Wennerstrom. Highly loaded axial flow compressors: History and current developments. *Journal of Turbomachinery*, 112(4):567–578, 1990.